American Journal of Transplantation 2005; 5: 58–67
Blackwell Munksgaard

doi: 10.1111/j.1600-6143.2004.00651.x

Selenium-Binding Protein-1 in Smooth Muscle Cells is Downregulated in a Rhesus Monkey Model of Chronic Allograft Nephropathy

Jose R. Torrealba[a], Matthew Colburn[b], Susan Golner[b], Zhen Chang[b], Tara Scheunemann[b], John H. Fechner[b], Drew Roenneburg[b], Huaizhong Hu[b], Tausif Alam[b], Hyoung T. Kim[b], Turan Kanmaz[b], Terry Oberley[a], Stuart J. Knechtle[b] and Majed M. Hamawy[b,*]

[a] *Department of Pathology and* [b] *Department of Surgery/Division of Transplantation, University of Wisconsin-Madison, WI*
* *Corresponding author: Majed M. Hamawy, hamawy@surgery.wisc.edu*

Treating patients with kidney failure by organ transplantation has been extraordinarily successful. Although, current immunosuppressants have improved short-term allograft survival, most transplants are eventually lost due to chronic allograft nephropathy (CAN). The molecular mechanisms underlying CAN are poorly understood. Smooth muscle cells (SMC) play a major role in the pathogenesis of CAN by contributing to the thickening of the intima and narrowing of the lumen of blood vessels. We show that selenium-binding protein-1 (SBP-1), a protein implicated in protein trafficking and secretion, is localized primarily to SMC *in vivo*. SBP-1 was heavily tyrosine-phosphorylated *in vivo*. Remarkably, SBP-1 was absent or strongly downregulated in vascular SMC in monkey kidney allografts with CAN. In contrast, the SMC α-actin was strongly expressed in the vascular SMC of the same allografts, indicating that the decrease in SBP-1 was not due to a global decrease in SMC proteins. Out of four growth factors implicated in the pathogenesis of CAN, only TGF-β blocked the expression of SBP-1; thus, TGF-β could regulate the expression of SBP-1 in CAN. These results show that SBP-1 localizes primarily to SMC *in vivo* and implicate this phosphoprotein in the effects of TGF-β on SMC and in the process of CAN.

Key words: Chronic allograft nephropathy, transplantation, smooth muscle, selenium-binding protein-1, vascular rejection, atherosclerosis

Received 9 June 2004, revised and accepted 10 August 2004

Introduction

Over the past few years, treating patients with kidney failure by solid-organ transplantation has been extraordinarily successful. Although current immunosuppressants have improved short-term graft survival, the majority of transplanted organs are eventually lost due to chronic allograft nephropathy (CAN) (1–3). The hallmarks of CAN are perivascular inflammation, fibrosis and chronic vascular rejection (allograft vasculopathy). Chronic vascular rejection is characterized by the thickening of the intima of the arteries and arterioles of the transplanted organ that leads to the narrowing of the lumen, ischemia and late graft failure. In contrast to classical atherosclerosis in which the manifestations are mostly focal and asymmetric (4), chronic vascular rejection is generalized, and the intimal thickening is concentric (5). Chronic vascular rejection is not specific for a certain organ, as it occurs in vascularized organ allografts, including kidney, heart, lung, liver and pancreas (6–8). The extent of vascular involvement varies, however, among different organs and in different donor-recipient combinations (9).

Smooth muscle cells (SMC) play an important role in intimal thickening and lumen narrowing, as the proliferation of these cells in the media, the layer beneath the intima, forces the endothelial layer inward (1–3). In addition, SMC migrate from the media to the intima where they proliferate and secrete matrix proteins (1–3). Leukocytes recruited in response to inflammation or injury also populate the thickened intima and may play a role in the activation and proliferation of SMC. Growth factors and cytokines, including PDGF, IFN-γ and TGF-β, released by resident cells and by infiltrating leukocytes have also been implicated in modulating SMC function and proliferation (10–13). Thus, controlling SMC processes should be important for controlling the thickening of the intima and, in turn, for regulating allograft rejection.

We used a rhesus monkey renal allograft model to identify molecules involved in CAN (14–17). We compared and contrasted the expression of tyrosine-phosphorylated proteins in naïve organs and rejected allografts using anti-phosphotyrosine Ab. We show that selenium-binding

protein-1 (SBP-1) (18–24), a protein implicated in the process of protein trafficking and secretion (25), is localized to SMC in normal tissues *in vivo*. We also demonstrate that this protein is strongly tyrosine-phosphorylated *in vivo*. Remarkably, SBP-1 was absent or strongly downregulated in vascular SMC in monkey allografts with CAN. In contrast, the SMC protein α-actin was strongly expressed in these rejected allografts. Out of four potent growth factors, only TGF-β blocked the expression of SBP-1 *in vitro*, thereby implicating this growth factor in controlling the level of SBP-1 *in vivo*. These results show that SBP-1 localizes primarily to SMC *in vivo* and implicate this phosphoprotein in the effects of TGF-β on SMC and in the process of CAN.

Materials and Methods

Human coronary artery, kidney and uterus samples

These samples were obtained at autopsy under an IRB exemption number E2002-108 and were used to determine the localization of SBP-1 *in situ*.

Cell lines

The normal human vascular (aorta) SMC cell line, CRL-1999, was obtained from ATCC (Manassas, VA). CRL-1999 cells were maintained in F12K Kaighn's modification media containing 10 mM TES, 0.3 mM L-ascorbic acid, 0.001 mM insulin, 0.001% Apo-transerrin, 58 nM sodium selenite, 0.003% endothelial growth supplement, 1% antibiotic/antimycotic, 1% L-glutamine, 1% HEPES, 1% non-essential amino acids, 1% sodium pyruvate and 10% heat-inactivated FCS. The cells were split once a week as per ATCC recommendation and were maintained for no more than ten divisions.

Ab production and purification

Rabbit sera to SBP-1 were generated by ProSci, Inc. (Poway, CA) and Biosource International, Inc. (Camarillo, CA). Rabbits were immunized with a cocktail of three peptides corresponding to different regions of SBP-1 in complete or incomplete Freund's adjuvant: peptide 1 (CDKQFYPDLIREGS); peptide 2 (CDFGKEPLGPALAHE) and peptide 3 (CRFYKNEGGTWSVEK). Anti-peptide response (titer) was monitored by enzyme-linked immunosorbent assay (ELISA), in which the plates were coated with the three peptides. Polyclonal Ab to each individual peptide were affinity purified using peptide-linked beads. Both anti-peptide 1 and anti-peptide 2 were immunogenic and mg concentrations of Ab were obtained. In contrast, peptide 3 was not immunogenic.

Graft transplant

The immunotoxin-treated rhesus monkey renal allograft model has previously been described (14–17). Donor-recipient pairs were selected on the basis of cytotoxic T-lymphocyte and mixed lymphocyte culture responses and major histocompatibility complex class I and class II typing. The donor left kidney was transplanted into recipients that had undergone bilateral native nephrectomy. The anti-CD3 immunotoxin FN18-CRM9 was administered to the monkeys as described previously (14,15,17). Although this therapeutic strategy prolongs allograft survival, most grafts develop signs of CAN, including severe interstitial fibrosis, tubular atrophy, chronic transplant glomerulopathy and chronic vasculopathy within 18 months after transplantation (14,15,17). Graft function was monitored by measuring serum creatinine levels, and rejection was biopsy confirmed. All animal procedures were approved by the University of Wisconsin Institutional Animal Care and Use Committee.

Tissue processing and two-dimensional (2-D) gel electrophoresis

Tissues were collected in ice-cold RPMI and minced into small pieces in urea buffer (8 M urea, 100 mM CHAPS, 2% pharmalyte 3–10 for IEF, 1% PMSF and 1% aprotinin) at a ratio of 1 g of tissue to 3 mL of urea buffer. After centrifugation, the supernatants were filtered in 100 kDa molecular weight cut-off filters and the flow-through samples were concentrated in 50 kDa molecular weight cut-off filters. Rehydration solution (8 M urea, 50 mM CHAPS, 0.3% bromphenol blue, 3 mM DTT and 0.08% IPG buffer pH 3–10) was combined with the samples at a ratio of 4:1, and used to rehydrate immobiline strips pH 3–10 (Amersham Biosciences, Piscataway, NJ) overnight at room temperature. The following day, the immobiline strips were subjected to isoelectric focusing (1-D) using the Multiphore II system (Amersham Biosciences), and then placed in SDS equilibration solution I (5% Tris–HCl pH 8.8, 6 M urea, 35% glycerol, 10% SDS, 0.2% bromophenol blue, and 3 mM DTT) for 15 min. After incubation, the immobiline strips were placed in SDS equilibration solution II (5% Tris–HCl pH 8.8, 6 M urea, 35% glycerol, 10% SDS, 0.2% bromophenol blue and 7 mM iodoacetamide) for an additional 15 min. Immobiline strips were then placed on the top of 10% Tris/glycine SDS-PAGE and held in place with 0.5% agarose overlay. The proteins in the strips were subjected to SDS-PAGE (2-D) and then transferred to PVDF membranes. Tyrosine-phosphorylated proteins were detected by blotting as described previously (26). Proteins were visualized using the LumiGLO kit (KPL, Gaithersburg, MD).

Mass spectrometry

Proteins from 2-D gel electrophoresis were visualized by coomassie blue staining. Two protein spots (~56 kDa) that were most strongly stained with commassie blue were excised and sent to the University of Wisconsin-Madison Biotechnology Center (Madison, WI) for Mass Spectrometry. All peptide masses 900–3200 Da were considered, and were analyzed using Matrix Science Mascot Peptide Mass Fingerprint (www.matrixscience.com). Locating phosphorylated proteins was accomplished by performing in-silica digest on SBP-1 using UCSF Protein Prospector program (MS Digest), and considering tyrosine phosphorylation as a modification. The in-silica digest-generated masses were compared against the 19 masses obtained through mass spectrometry.

Light microscopy

Routine light microscopy on hematoxylin and eosin (H&E) stained sections were performed on paraffin-embedded tissues or frozen sections. Kidney specimens with at least one glomerulus and one blood vessel were considered appropriate for evaluation. The Banff criteria of kidney transplant pathology was used for scoring the presence and degree of rejection (27). CAN was defined by the presence of interstitial fibrosis, tubular atrophy, allograft glomerulopathy, mesangial matrix increase and vascular fibrous intimal thickening.

Immunohistochemistry

Immunohistochemical labeling was performed on snap frozen specimens and on selected paraffin-embedded tissues. For frozen sections, 5-μm sections were obtained from each tissue block and fixed in cold acetone and stored at −20°C. The slides were then dried at 37°C for 30 min and fixed in acetone for 5 min at room temperature. Selected tissues were processed for routine paraffin embedding. Five-micron sections were obtained from each tissue block, deparaffinized in xylene and rehydrated through graded ethanol to water. The slides were subjected to heat-induced epitope retrieval in 10 mM EDTA solution using a decloaking chamber (Biocare Medical, Walnut Creek, CA) at 6 psi for 45 min. The slides were rinsed with TBS/Tween and the non-specific sites were blocked by using a casein-based blocking agent (Sniper, Biocare Medical). Purified polyclonal rabbit Ab against two different peptides of SBP-1 (1:200 dilution) were used to incubate the slides for 1 h at room temperature. As a control, specimens were also stained with anti-α-actin monoclonal Ab (Sigma, St. Louis, MO; 1:45000 dilution). After rinsing with TBS/Tween, the slides were treated with synthetic polymer Envision Plus HRP system (Dakocytomation, Carpinteria, CA). After incubation, the slides were washed with TBS/Tween and incubated with DAB chromagen (Dakocytomation) for 5 min. Following incubation, they were counterstained with hematoxylin, dehydrated,

cleared and cover slipped. Blood vessels from naïve and experimental animals immunolabaled with anti-SBP-1 Ab were scored using a semi-quantitative scale (0–3): 0 = no staining, +1 = mild, +2 = moderate, +3 = strong.

Reverse transcription polymerase chain reaction (RT-PCR)

Total RNA was extracted using the SV Total RNA Isolation System (Promega, Madison, WI) (26). The resultant mRNA was reverse transcribed to generate first-strand cDNA using avian myeloblastosis virus reverse transcriptase. SBP-1 cDNA was amplified using PCR with the SBP-1-specific oligonucleotides 5′-AAGTGCTGGAGGACGAGGAAC-3′ (sense) and 5′-AAAATAGGGAGTGTGGGTGAT-3′ (antisense). The anti-sense primer corresponds to the 3′-untranslated region of SBP-1. β-actin cDNA was amplified with 5′-CCCAAGGCCACCGCGAGAAGAT-3″ (sense) and 5′-GTCCCGGCCAGCCAGGTCCAG-3′ (anti-sense). PCR products were then subjected to 1% agarose gel electrophoresis and visualized by ethidium bromide staining.

Statistical analysis

The biopsies were divided into two categories: normal and rejection. To examine differences in staining scores across diagnostic groups, a non-parametric one-way ANOVA was performed by analyzing the ranked SBP-1 staining scores. Statistical analysis was performed using SAS v. 6.12 for Windows (SAS Institute, Cary, NC).

Results

Isolation of a 56-kDa tyrosine-phosphorylated protein from kidneys

We chose to look for tyrosine-phosphorylated proteins because these proteins control the function and growth of all cells. To identify tyrosine-phosphorylated proteins involved in the process of CAN, kidney lysates from naïve kidneys and from allograft kidneys with CAN were subjected to 2-D gel electrophoresis. Proteins were transferred to PVDF membranes, and then immunoblotted with anti-phosphotyrosine Ab. As shown in Figure 1A, ~56-kDa tyrosine-phosphorylated proteins were reproducibly and prominently present in naïve kidneys. These protein spots were not detected in rejected allograft kidneys (see below). We had to try numerous homogenization procedures, solubilization buffers and filtration procedures to be able to detect distinct protein spots upon blotting the membranes with anti-phosphotyrosine Ab. We found that homogenizing the tissues in urea buffer, filtering the lysates through a 100 kDa molecular weight cut-off filters, and then washing and concentrating the flow-through samples in 50 kDa molecular weight cut-off filters to be critical to obtain distinct unsmeared tyrosine-phosphorylated spots. Although exposing the membrane in Figure 1A to films for only a few minutes led to the appearance of prominent 56-kDa spots, exposing the same membrane to films for extended time also led to the appearance of other tyrosine-phosphorylated spots (not shown). Because the 56-kDa protein spots were prominent in the membranes, and because their level in naïve kidneys was different from rejecting kidney allografts we chose to concentrate our effort on identifying the 56-kDa protein spots.

Identification of the 56-kDa tyrosine-phosphorylated protein as SBP-1

Proteins in tissue lysates from monkey kidneys were subjected to 2-D gel electrophoresis as described above, and then stained with commassie blue. Two spots corresponding to the ~56-kDa proteins that were most strongly

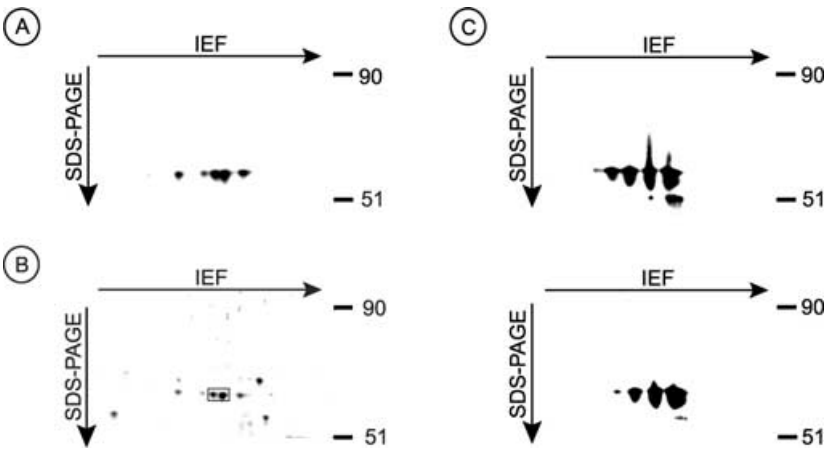

Figure 1: The identification of a 56-kDa heavily tyrosine-phosphorylated protein in monkey kidneys as SBP-1. (A) Normal monkey kidneys were homogenized in urea buffer and the lysates were then centrifuged at room temperature for 30 min. The supernatants were filtered in 100 kDa molecular weight cut-off filters and the flow-through samples were washed and concentrated in 50 kDa molecular weight cut-off filters. The samples were then subjected to 2-D gel electrophoresis. The proteins were transferred to PVDF membranes, and tyrosine-phosphorylated proteins were detected by blotting with HRP-conjugated anti-phosphotyrosine antibodies PY-20. Proteins were visualized using the LumiGLO kit. (B) Kidney lysates prepared as above were subjected to 2-D gel electrophoresis and the gel was stained with Coomassie Blue. Box indicates the two protein spots that were most strongly stained with Commassie Blue; both spots were analyzed by mass spectrometry. (C) Kidney lysates prepared as above were subjected to 2-D gel electrophoresis. The proteins were transferred to PVDF membranes and were labeled by blotting with anti-SBP-1 polyclonal Ab (upper panel). The Ab were then stripped and reblotted with HRP-conjugated anti-phosphotyrosine Ab PY-20 (lower panel).

stained with commassie blue (Figure 1B; see box) were excised from the gel and were sent to the University of Wisconsin-Madison Biotechnology Center for mass spectrometry. In-gel trypsin digest yielded 19–21 peptides from each of the protein spots, of which at least 15 masses exactly matched SBP-1 covering 41% of the protein ($p < 0.05$). Thus, the 56-kDa tyrosine-phosphorylated protein is the previously known protein SBP-1 (18–23). To identify the tyrosine residues in SBP-1 that are phosphorylated, in-silica digest of SBP-1 was performed using the UCSF Protein Prospector program. Protein tyrosine phosphorylation was a considered modification. The in-silica digest-generated masses were compared to the peptide masses obtained through mass spectrometry. Two masses showed tyrosine phosphorylation modification: mass 1454.6 (QYDISDPQRPR) and mass 1849.7 (CGNCGPGYSTPLEAMK) indicated that tyrosine 12 and tyrosine 335, respectively, were phosphorylated. To further examine tyrosine phosphorylation of SBP-1, proteins in kidney lysates were subjected to 2-D electrophoresis, transferred to PVDF membranes, and then immunoblotted with anti-SBP-1 Ab (Figure 1C, upper panel). The anti-SBP-1 Ab were then striped off and the membranes were reimmunoblotted with anti-phosphotyrosine Ab (Figure 1C, lower panel). As shown in Figure 1C, identical spots were detected by both Ab, confirming that SBP-1 is tyrosine-phosphorylated *in vivo*.

SBP-1 localizes to SMC in vivo

To determine the localization of SBP-1 *in vivo*, we immunolabeled monkey kidney tissues with anti-SBP-1 Ab. SBP-1 staining was localized to the vascular SMC of the blood vessels (Figure 2). Incubating anti-SBP-1 Ab for 30 min with blocking peptides (peptides used to generate the Ab) before immunostaining blocked SMC staining in a dose-dependent manner, confirming the specificity of the Ab (Figure 2, compare B with C and D).

To rule out the possibility that these results are limited to a certain tissue or animal species, we also stained various tissues from different animal species with two anti-SBP-1 Ab that recognize two different sites of the molecule. In all the tissues examined, SBP-1 was localized to the SMC cells (Figure 3). SBP-1 was not detected in cardiac muscles (Figures 3A–C) or skeletal muscles (Figure 3G). However, in the uterus SBP-1 was detected in vascular SMC and uterine SMC (Figure 3H), indicating that this protein is not specific to vascular SMC but is also found in SMC of other tissues. Note that two Ab that recognize two different sites of SBP-1 showed that SBP-1 is localized to SMC: All tissues in Figures 2 and 3 were stained with anti-SBP-1 Ab that recognize the SBP-1 peptide sequence (CDFGKEPLGPALAHE), except for the tissues in Figures 3C, F and I, which were stained with anti-SBP-1 Ab that recognize the SBP-1 peptide sequence (CDKQFYPDLIREGS).

To confirm that SBP-1 is found in SMC, aortas from monkeys were subjected to 2-D electrophoresis, the proteins were transferred to PVDF membranes, and then immunoblotted with anti-SBP-1 Ab. SBP-1 was detected in the lysates of the aorta, confirming the presence of this protein in blood vessels (Figure 4A). As shown in Figure 4B, SBP-1 was also strongly expressed in the primary SMC line, CRL-1999, confirming the expression of this protein in SMC. Some of SBP-1 in tissues appears to have isoelectric point different from SBP-1 in the CRL-1999 cells (compare Figures 4A and B). This is most likely due to differences in posttranslation modification of SBP-1 in tissues vs in cells grown *in vitro*.

Interestingly, most of SBP-1 in the CRL-1999 cells localized to the detergent-insoluble fraction that contains the nucleic material and cytoskeleton-associated molecules (Figure 5). Boiling the insoluble fraction in sample buffer with vigorous vortexing led to the release of SBP-1 (Figure 5). Changing the detergent (Figure 5) or the concentration of the detergent (not shown) did not increase the solubility of the protein.

SBP-1 is downregulated in kidney allografts with CAN

As described above, we became interested in the 56-kDa protein because it was absent in tissues obtained from rejecting animals. The monkey model that we used here has previously been described in detail (14–17). In this model, most of the allografts develop signs of CAN, including severe interstitial fibrosis, tubular atrophy, chronic transplant glomerulopathy and chronic vascular rejection

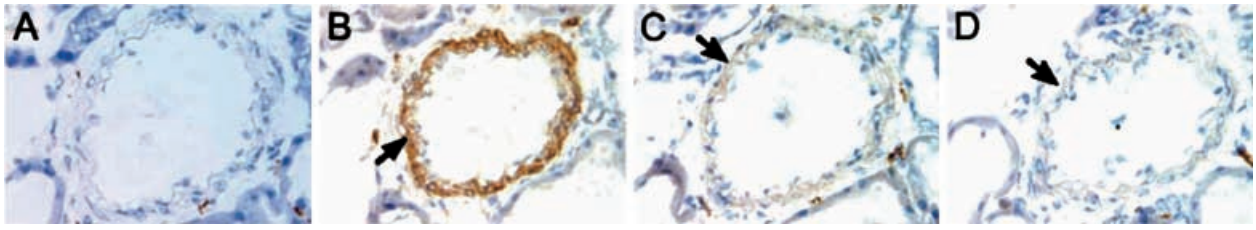

Figure 2: Localization of SBP-1 to SMC *in vivo*. Immunohistochemical labeling was performed using normal rabbit serum (A) or affinity purified rabbit polyclonal anti-SBP-1 Ab (B)–(D). (A; 400×) normal monkey kidney; (B; 400×) normal monkey kidney; (C; 400×) normal monkey kidney (stained in the presence of 10 μg of blocking peptide); (D; 400×) normal monkey kidney (stained in the presence of 20 μg of blocking peptide). Arrow indicates vascular SMC.

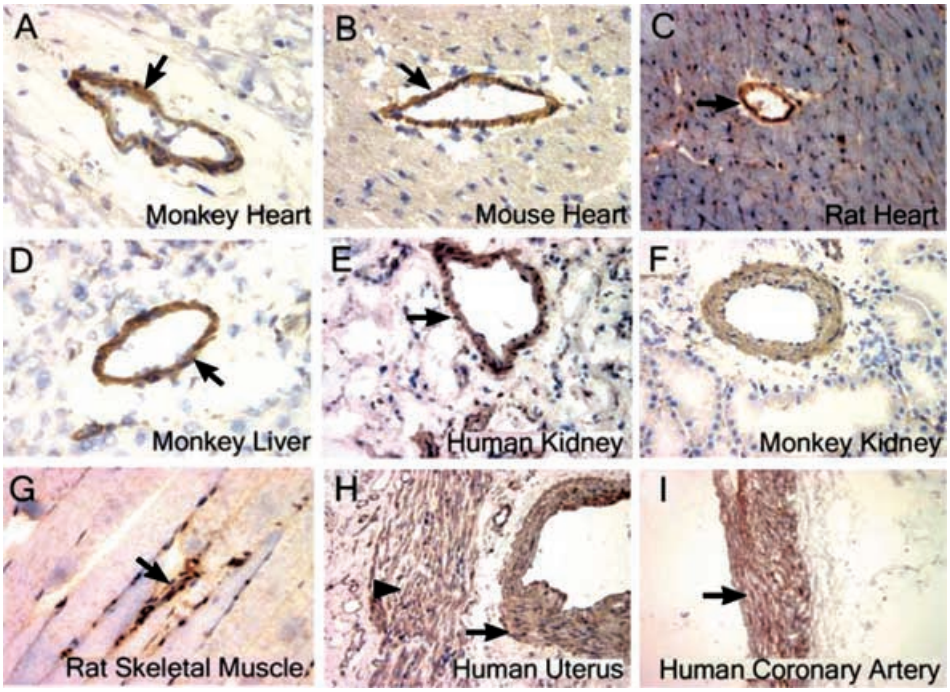

Figure 3: SBP-1 is localized primarily to SMC *in vivo*. Immunohistochemical labeling was performed using affinity purified rabbit polyclonal anti-SBP-1 Ab (A)–(I). (A; 400×) normal monkey heart; (B; 400×) normal mouse heart; (C; 200×) normal rat heart; (D; 400×) normal monkey liver; (E; 400×) normal human kidney; (F; 400×) normal monkey kidney; (G; 400×) normal rat skeletal muscle; (H; 200×) normal human uterus; (I; 100×), normal human coronary artery. (A)–(I) were stained with anti-SBP-1 Ab (anti-peptide 2) except (C, F and I), which were stained with anti-SBP-1 Ab (anti-peptide 1). Arrow indicates vascular SMC; arrowhead indicates uterine SMC.

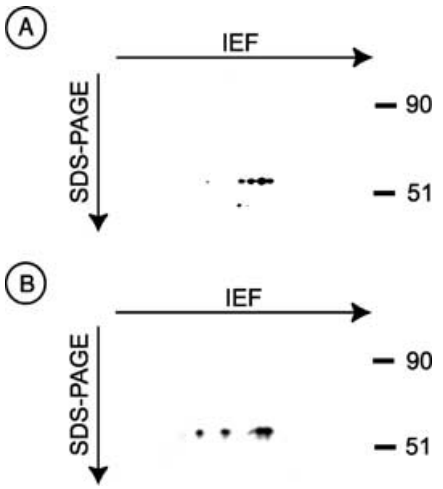

Figure 4: Detection of SBP-1 in aorta and in the SMC cell line CRL-1999. (A) Normal monkey aorta was homogenized in urea buffer and the lysates were then centrifuged at room temperature for 30 min. The supernatants were filtered in 100 kDa molecular weight cut-off filters and the flow-through samples were washed and concentrated in 50 kDa molecular weight cut-off filters. The samples were then subjected to 2-D gel electrophoresis. The proteins transferred to PVDF membranes, and SBP-1 was detected by blotting with anti-SBP-1 Ab followed by HRP-conjugated secondary Ab. Proteins were visualized using the LumiGLO kit. (B) CRL-1999 cells were solubilized with urea buffer and subjected to 2-D gel electrophoresis. SBP-1 was detected as described in (A).

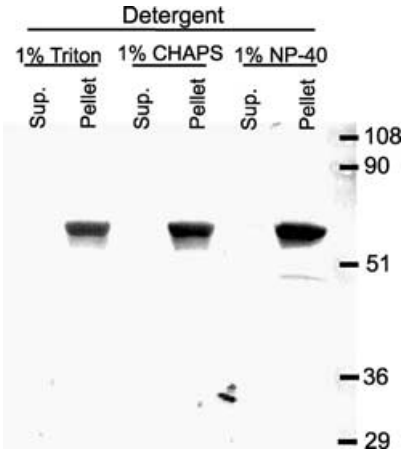

Figure 5: SBP-1 localizes to detergent-insoluble fractions. CRL-1999 cells were lysed for 30 min with ice-cold lysis buffer containing the detergents 1% Triton X-100, 1% CHAPS or 1% NP-40. Cell lysates were centrifuged at 4°C for 30 min. Supernatants were removed, and filtered through 100 kDa molecular weight cut-off filters and the flow-through samples were then concentrated in 30 kDa molecular weight cut-off filters. An equal volume of 2× sample buffer was added to the concentrated supernatants, and boiled for 30 min. Meanwhile, the pellets were solubilized in 1× sample buffer and boiled for 30 min. Supernatants and pellets were subjected to SDS-PAGE. Proteins were transferred to PVDF membranes and blotted with anti-SBP-1 Ab followed with HRP-conjugated secondary Ab. Proteins were visualized using the LumiGLO kit.

within 18 months after transplantation. Chronic vascular rejection was characterized by fibrointimal proliferation and narrowing of vascular lumen due to proliferation of SMC, fibroblasts, myofibroblasts and deposition of extracellular matrix proteins (14,15,17).

To examine the involvement of SBP-1 in allograft rejection, tissues from naïve (normal untransplanted) monkey kidneys and from allograft monkey kidneys with CAN were subjected to SDS-PAGE. The proteins were transferred to PVDF membranes and then immunolabeled with anti-SBP-1 Ab. As shown in Figure 6, SBP-1 was strongly expressed in kidneys obtained from naïve but not from rejected allograft kidneys. Immunoblotting with anti-α-actin Ab showed strong α-actin levels in all lanes (Figure 6).

To further examine these results, we performed immunohistochemistry on naïve monkey kidneys and on monkey kidney allografts with CAN. Figure 7 shows the results from a representative naïve kidney (A–C) and from a kidney allograft with CAN (D–I). The sections were stained with H&E (A, D, G), immunolabeled with anti-SMC α-actin Ab (B, E, H), or immunolabeled with anti-SBP-1 Ab (C, F, I). Note that each set of images (A–C), (D–F) and (G–I) depict the same blood vessel. H&E staining of kidneys with CAN showed blood vessels with chronic vascular rejection, including thickening of the intima and a significant narrowing of the lumen (Figure 7D and G). Both α-actin (Figure 7B) and SBP-1 (Figure 7C) were strongly labeled in the vascular SMC of the naïve kidney. In contrast, α-actin

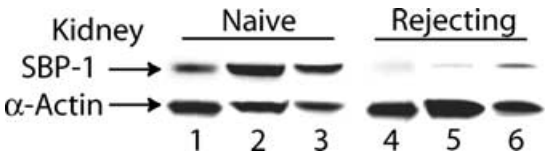

Figure 6: Downregulation of SBP-1 in rejected allografts with CAN. Biopsies from naïve kidneys (lanes 1, 2 and 3) and from rejected allograft kidneys (lanes 4, 5 and 6) were subjected to SDS-PAGE. Proteins were transferred to PVDF membranes and blotted with anti-SBP-1 Ab or anti-α-actin Ab followed with HRP-conjugated secondary Ab. Proteins were visualized using the LumiGLO kit.

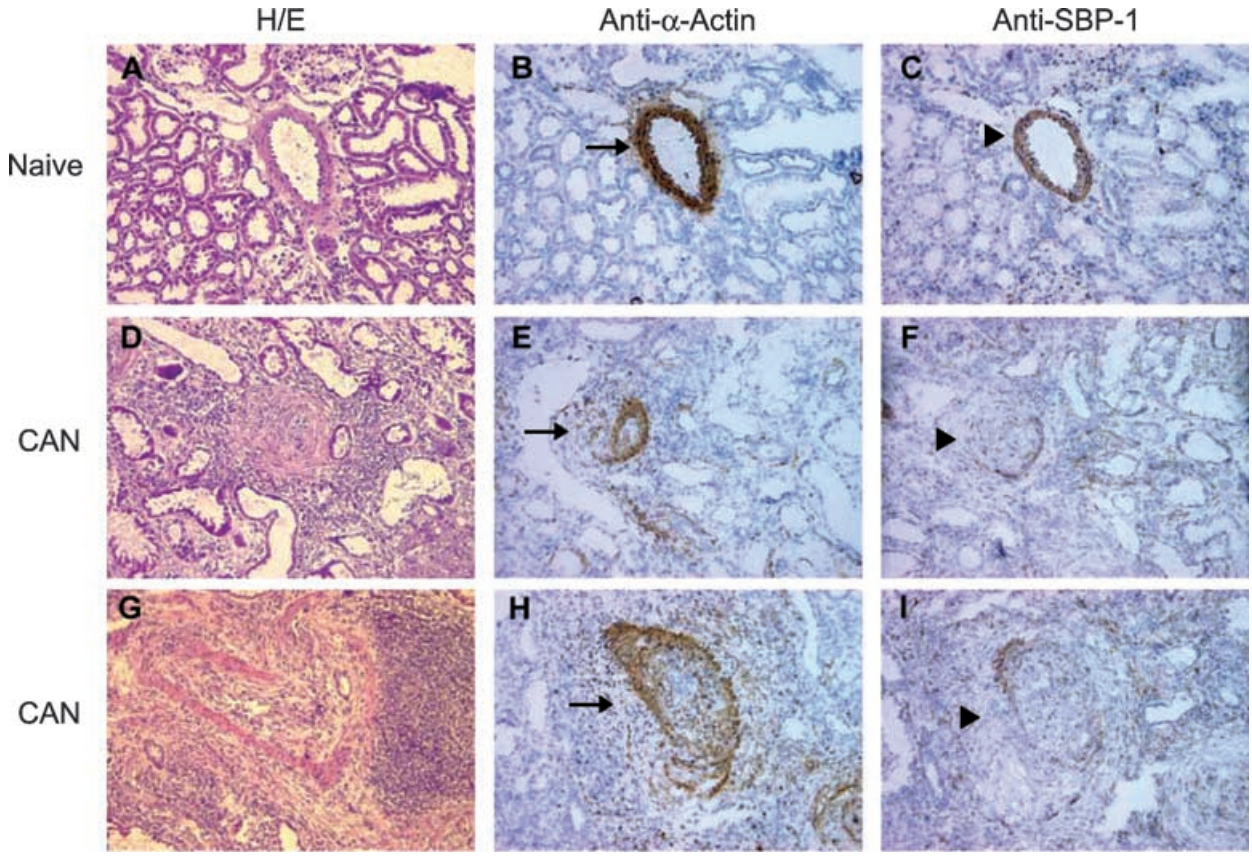

Figure 7: SBP-1 is downregulated in allograft kidneys with CAN. Immunohistochemical staining of a representative naïve monkey kidney (A–C; 200×) and of a monkey kidney allograft with CAN (D–I; 200×). The sections were stained with H&E (A, D, G), immunolabeled with anti-α-actin Ab (B, E, H), or immunolabeled with anti-SBP-1 Ab (C, F, I). Arrows indicate blood vessels labeled with anti-α-actin Ab; Arrowheads indicate the same vessels labeled with anti-SBP-1 Ab.

(Figure 7E and H) but not SBP-1 (Figure 7F and I) was strongly expressed in the SMC of blood vessels with chronic vascular rejection, as SBP-1 labeling was weak or undetectable.

To analyze these results statistically, tissues from 5 naïve kidneys (5 monkeys) and from 14 rejected kidney allografts (14 monkeys) showing a spectrum of chronic vascular rejection changes were immunohistochemically labeled with anti-SBP-1 Ab and a semi-quantitative scale from 0 to +3 was used to grade the intensity of vascular SMC staining. SBP-1 staining was significantly ($p < 0.0001$) weaker in kidney blood vessels with chronic rejection compared to normal blood vessels in naïve kidney (Table 1).

TGF-β downregulates the expression of SBP-1

Graft rejection is characterized by a marked increase in the level of an array of growth factors (1–3). Some of these factors have been shown to regulate the expression of molecules (10–13). We reasoned that the decrease in the level of SBP-1 in the SMC of rejecting grafts might be due to a growth-factor(s)-induced signal. We determined the effect of TGF-β, IFN-γ, TNF-α and PDGF on the expression of SBP-1 in the primary SMC line CRL-1999. Under the conditions used in our studies, only TGF-β led to a sharp decline in SBP-1 mRNA, which was time (Figure 8A) and dose (Figure 8B) dependent. Varying the concentrations of IFN-γ, TNF-α, and PDGF did not alter SBP-1 expression (not shown). SBP-1 mRNA level declined within 3 days after TGF-β treatment and was completely absent in most experiments within 2 weeks. TGF-β did not alter the level of β-actin mRNA, which is consistent with previous reports (10,11). Incubating the cells for 14 days with TGF-β induced only a modest decrease in the level of the SBP-1 protein (Figure 8C); thus, SBP-1 protein is relatively stable *in vitro*. In contrast, the level of SMC α-actin protein increased by TGF-β, which is also consistent with previously published reports (10,11). Notably, incubating the cells for 14 days with TGF-β at conditions that lead to the decrease in SBP-1 level increased the number of SMC (Table 2). Cell viability in these studies were at least 95% as determined by Trypan Blue exclusion (not shown).

Table 1: Semi-quantitative analysis of SBP-1 staining in vascular SMC of naïve blood vessels and of blood vessels with chronic vascular rejection

Kidney diagnosis (Banff)	No. of cases	SBP-1 staining intensity
Naïve	5	+3, +3, +3, +3, +3
AR I-CAN I	2	+1,+1
AR I-CAN II	2	+1,+1
AR II-CAN I	1	+1
AR II-CAN II	2	+1,+1
AR II-CAN III	2	0,0
AR III-CAN I	1	0
AR III-CAN II	1	0
CAN I	1	+2
CAN II	1	+1
CAN III	1	+1

0 = No staining; 1 = mild staining; 2 = moderate staining; 3 = strong staining; AR = acute rejection; CAN = chronic allograft nephropathy.

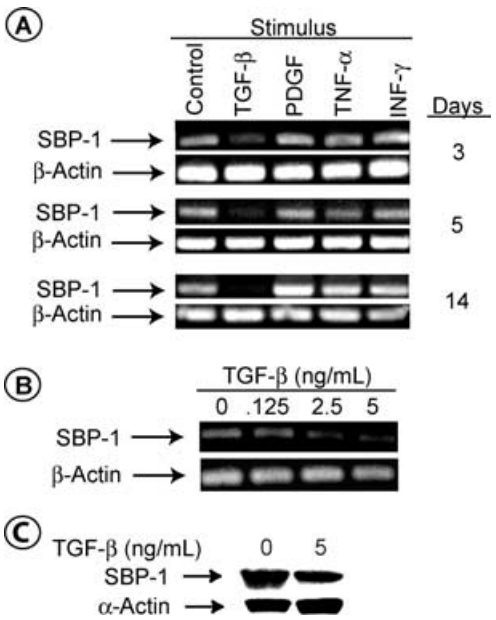

Figure 8: TGF-β downregulates the expression of SBP-1. (A) 1×10^5 CRL-1999 cells in F12K Kaighn's modification media were plated in 100 mm tissue culture dishes for 24 h at 37°C. After incubation, 5 ng/mL TGF-β, 1 ng/mL TNF-α, 50 ng/mL IFN-γ or 10 ng/mL PDGF was added to the dishes and the incubation resumed for indicated time at 37°C. The cells were then detached from the plates with trypsin, washed in PBS, and counted. Total RNA was extracted then reverse transcribed to generate first-strand cDNA using avian myeloblastosis virus reverse transcriptase. cDNA was then amplified using PCR with the SBP-1 or β-actin oligonucleotides. PCR products were subjected to 1% agarose gel electrophoresis and visualized by ethidium bromide staining. (B) CRL-1999 cells were grown as described above in the presence of the indiacted concentration of TGF-β for 14 days at 37°C. Total RNA was extracted and PCR products were generated as described above. (C) CRL-1999 cells were incubated with the indicated concentrations of TGF-β for 14 days at 37°C. The cells were detached, counted, and then lysed with ice-cold 1× lysis buffer. Cell lysates were centrifuged at 4°C for 30 min. Supernatants were removed, the pellets were solubilized in 1× sample buffer, boiled for 30 min, and then subjected to SDS-PAGE. Proteins were transferred to PVDF membranes and blotted with anti-SBP-1 Ab or anti-α-actin Ab followed with HRP-conjugated secondary Ab. Proteins were visualized using the LumiGLO kit.

Table 2: TGF-β induces proliferation of CRL-1999 cells (n = 8)

TGF-β (ng/mL)	Increase from untreated cells (mean ± SD) (%)
0.5	66 ± 33
5	81 ± 42
10	111 ± 35

Discussion

CAN is a major cause of allograft failure in clinical renal transplantation. Yet, the molecular mechanisms underlying CAN are poorly understood. Indeed, identifying the molecules involved in CAN is important for understanding the molecular mechanisms underlying CAN, and for designing therapeutic strategies to prolong allograft survival. SMC play an important role in the pathogenesis of CAN by contributing to the thickening of the intima and the loss of lumen. We showed in this paper that the phosphoprotein SBP-1 is localized primarily to SMC *in vivo*. We also showed in a well-established rhesus monkey renal transplant model that the level of SBP-1 dramatically decreased in the vascular SMC of allografts with CAN. In contrast, the SMC protein α-actin was strongly expressed in the same SMC, thereby indicating that the decrease in SBP-1 is not due to a global decrease in the level of proteins in SMC of blood vessels with chronic rejection.

SBP-1 has been shown to regulate vesicular transport in an intra-golgi transport cell-free assay *in vitro* (25). Because intra-golgi transport is critical for protein processing and packaging, SBP-1 appears to play a role in regulating protein trafficking and secretion. However, in these *in vitro* studies only 10% of SBP-1 associated with the Golgi apparatus. SBP-1 has also been shown to bind selenium *in vitro* (18). Selenium is a trace element critical for a number of biological processes, including optimal SMC growth *in vitro* (28–33). Interestingly, the transport activity of SBP-1 was independent of its ability to bind selenium (25), thereby suggesting that SBP-1 may function in multiple cellular processes. Our cell solubilization studies with detergents suggested that SBP-1 might be a cytoskeleton-associated protein (Figure 5). Accordingly, SBP-1 has been shown to localize with G-actin at the cell margins of transformed cell lines (24). We also showed here that SBP-1 is tyrosine-phosphorylated *in vivo*. Given that tyrosine phosphorylation is an important process by which proteins interact, our results suggest that SBP-1 might function as a linker molecule involved in protein interaction. Together, these studies implicate SBP-1 in playing a role in important cellular processes.

Our immunohistochemical studies showed that SBP-1 is localized primarily to SMC *in vivo*. Previous studies examined the expression of SBP-1 by looking for SBP-1 mRNA in total RNA extracts or by immunoblotting whole tissue lysates with anti-SBP-1 Ab (18–23). Thus, because all tissues contain blood vessels, it is not surprising that in those studies SBP-1 mRNA and protein were present in the extracts and lysates of a variety of tissues. At the time this manuscript was being prepared for publication, Chen et al. reported nuclear SBP-1 staining of normal epithelial cells. They also reported that the expression of cytoplasmic SBP-1 was increased in well-differentiated adenocarcinoma, but decreased in poorly differentiated adenocarcinoma (34). Their figures did not contain blood vessels and there was no mention of the expression of SBP-1 in vascular SMC. We found, using anti-SBP-1 Ab that recognize two different parts of SBP-1, that this protein is localized to SMC *in vivo* in normal subjects. We did not detect any SBP-1 nuclear staining in any of the tissues we examined. SBP-1 has also been recently shown to be located at the leading edges of rapidly growing protrusions and growing tips of the cultured transformed cells lines T98G glioma cells and SH-SY5y neuroblastoma cells (24). We did not examine the presence of this protein in transformed tissues and cells, as this issue is beyond the scope of this manuscript.

TGF-β strongly downregulated the level of SBP-1 *in vitro* (Figure 8), suggesting that this growth factors might regulate the level of SBP-1 *in vivo*. TGF-β has been implicated in the pathogenesis of allograft vasculopathy (35,36). Accordingly, anti-TGF-β Ab has been shown to reduce intimal hyperplasia (36). SMC would be exposed to TGF-β following injury to the endothelium (37). Platelets, endothelial cells, and infiltrating cells such as macrophages and lymphocytes all produce TGF-β. Therefore, at the time of inflammation and tissue injury, SMC are exposed to TGF-β from different sources.

TGF-β has been shown to regulate SMC processes *in vitro* (10,37–42). These TGF-β effects were dependent on the culture conditions and the SMC cell line used. In our studies, TGF-β at conditions that lead to the decrease in SBP-1 level increased the number of SMC (Table 2). The relationship between the decrease in SBP-1 level and the increase in SMC number is not clear at this time. TGF-β has been shown to exert some of its effects by inducing the release of growth factors such as PDGF from SMC (38). However, our data showed that exogenous PDGF did not affect the level of SBP-1 in SMC.

SMC play an important role in the pathogeneses of chronic vascular rejection and in turn in CAN. The increased proliferation of SMC has been implicated in playing a major role in causing the thickening of the intima and the narrowing of the lumen in chronic vascular rejection. Our studies showed that in cells treated with TGF-β there was an inverse relationship between the level of cellular SBP-1 and cell proliferation, thereby suggesting that SBP-1 might be involved in regulating cell proliferation. Thus, it is possible that under normal situations SBP-1 keeps SMC proliferation in check, and that the decrease in its level leads to enhanced cell proliferation. Accordingly, the increase in TGF-β in CAN leads to the decrease in SBP-1, which in turn leads to SMC proliferation. Thus, SBP-1 might play a protective role in CAN by keeping SMC proliferation in check. This is an issue that awaits further investigation.

In summary, we have shown that SBP-1 is a tyrosine-phosphorylated protein localized primarily to SMC *in vivo*. The localization of SBP-1 to SMC *in vivo* suggests that

SBP-1 plays a role in processes important to SMC. SBP-1 expression was also downregulated by TGF-β, an important player in the pathogenesis of CAN. SBP-1 expression was absent or markedly reduced in vascular SMC of rejected monkey allografts with CAN. The precise contribution of SBP-1 to the process of CAN awaits further investigation.

Acknowledgement

We thank Dr Glen Leverson and Mr Alejandro Munoz-del-Rio for the statistical analyses of the results.

References

1. Paul LC, Fellstrom B. Chronic vascular rejection of the heart and the kidney—Have rational treatment options emerged? Transplantation 1992; 53: 1169–1179.
2. Libby P, Pober JS. Chronic rejection. Immunity 2001; 14: 387–397.
3. Womer KL, Vella JP, Sayegh MH. Chronic allograft dysfunction: Mechanisms and new approaches to therapy. Semin Nephrol 2000; 20: 126–147.
4. Glass CK, Witztum JL. Atherosclerosis: The road ahead. Cell 2001; 104: 503–516.
5. Foegh ML. Chronic rejection—Graft arteriosclerosis. Transplantation Proc 1990; 22: 119–122.
6. Yousem SA, Paradis IL, Dauber JH et al. Pulmonary arteriosclerosis in long-term human heart-lung transplant recipients. Transplantation 1989; 47: 564–569.
7. Demetris AJ, Markus BH, Burnham J et al. Antibody deposition in liver allografts with chronic rejection. Transplantation Proc 1987; 19: 121–125.
8. Sibley RK, Sutherland DER. Pancreas transplantation—an immunohistologic and histopathologic examination of 100 grafts. Am J Pathol 1987; 128: 151–170.
9. Cramer DV, Qian SQ, Harnaha J et al. Cardiac transplantation in the rat. I: The effect of histocompatibility differences on graft arteriosclerosis. Transplantation 1989; 47: 414–419.
10. Hautmann MB, Madsen CS, Owens GK. A TGF-β control element drives TGF-β induced stimulation of smooth muscle α-actin gene expression in concert with twl CArG elements. J Biol Chem 1997; 272: 10948–10955.
11. Hautmann MB, Adam PJ, Owens GK. Similarities and differences in smooth muscle α-actin induction by TGF-β in smooth muscle versus non-smooth muscle cells. Arteriocler Thromb Vasc Biol 1999; 19: 2049–2058.
12. Bjorkerud S. Effects of TGF-β-1 on human arterial smooth-muscle cells *in vitro*. Arterioscler Thromb 1991; 11: 892–902.
13. Kato Y, Periasamy M. Growth and differentiation of smooth muscle cells during vascular development. Trends Cardiovasc Med 1996; 6: 100–106.
14. Lagoo AS, Buckley PJ, Burchell LJ et al. Increased glomerular deposits of von Willebrand factor in chronic, but not acute, rejection of primate renal allografts. Transplantation 2000; 70: 877–886.
15. Torrealba J, Fernandez LA, Kanmaz T et al. Immunotoxin-treated rhesus monkeys: A model for renal allograft chronic rejection. Transplantation 2003; 76: 524–530.
16. Thomas JM, Neville DM, Contreras JL et al. Preclinical studies of allograft tolerance in rhesus monkeys: A novel anti-CD3-immunotoxin given peritransplant with donor bone marrow induces operational tolerance to kidney allografts. Transplantation 1997; 64: 124–135.
17. Knechtle SJ, Fechner JH Jr, Dong Y et al. Primate renal transplants using immunotoxin. Surgery 1998; 124: 438–447.
18. Bansal MP, Mukhopadhyay T, Scott J et al. DNA sequencing of a mouse liver protein that binds selenium: Implications for selenium's mechanism of action in cancer prevention. Carcinogenesis 1990; 11: 2071–2073.
19. Giometti CS, Liang X, Tollaksen SL et al. Mouse liver selenium-binding protein decreased in abundance by peroxisome proliferators. Electrophoresis 2000; 21: 2162–2169.
20. Lanfear J, Fleming J, Walker M, Harrison P. Different patterns of regulation of the genes encoding the closely related 56-kDa selenium- and acetaminophen-binding proteins in normal tissues and during carcinogenesis. Carcinogenesis 1993; 14: 335–340.
21. Jamba L, Nehru B, Medina D, Bansal MP, Sinha R. Isolation and identification of selenium-labeled proteins in the mouse kidney. Anticancer Res 1996; 16: 1651–1657.
22. Yang M, Sytkowski AJ. Differential expression and androgen regulation of the human selenium-binding protein gene hSP56 in prostate cancer cells. Cancer Res 1998; 58: 3150–3153.
23. Chang PW, Tsui SK, Liew C, Lee CC, Waye MM, Fung KP. Isolation, characterization, and chromosomal mapping of a novel cDNA clone encoding human selenium binding protein. J Cell Biochem 1997; 64: 217–224.
24. Miyaguchi K. Localization of selenium-binding protein at the tips of rapidly extending protrusions. Histochem Cell Biol 2004; 121: 371–376.
25. Porat A, Sagiv Y, Elazar Z. A 56-kDa selenium-binding protein participates in intra-golgi protein transport. J Biol Chem 2000; 275: 14457–14465.
26. Peters D, Tsuchida M, Manthei ER et al. Potentiation of CD3-induced expression of the linker for activation of T cells (LAT) by the calcineurin inhibitors cyclosporin A and FK506. Blood 2000; 95: 2733–2741.
27. Racusen LC, Solez K, Colvin RB. The Banff 97 working classification of renal allograft pathology. Kidney Int 1999; 55: 713–723.
28. Behne D, Kyriakopoulos A. Mammalian selenium-containing proteins. Annu Rev Nutr 2001; 21: 453–473.
29. Combs GF Jr, Gray WP. Chemopreventive agents: Selenium. Pharmacol Ther 1998; 79: 179–192.
30. Ip C. Lessons from basic research in selenium and cancer prevention. J Nutr 1998; 128: 1845–1854.
31. Flohe L, Andreesen JR, Brigelius-Flohe R, Maiorino M, Ursini F. Selenium, the element of the moon, in life on earth. IUBMB Life 2000; 49: 411–420.
32. Medina D. Mechanisms of selenium inhibition of tumorigenesis. J Am Coll Toxicol 1987; 5: 21–27.
33. Ip C. The chemopreventive role of selenium in carcinogenesis. J Am Coll Toxicol 1987; 5: 7–20.
34. Chen GA, Wang H, Miller CT et al. Reduced selenium-binding protein I expression is associated with poor outcome in lung adenocarcinomas. J Pathol 2004; 202: 321–329.
35. Mallat Z, Tedgui A. The role of TGF-β in atherosclerosis: Novel insights and future perspectives. Curr Opin Lipidol 2002; 13: 523–529.
36. Wolf YG, Rasmussen LM, Ruoslahti E. Antibodies against TGF-β-1 suppress intimal hyperplasia in a rat model. J Clin Invest 1994; 93: 1172–1178.
37. Battegay EJ, Raines EW, Selfert RA, Bowen-Pope DF, Ross R. TGF-β induces bimodal proliferation of connective tissue cells via complex control of an autocrine PDGF loop. Cell 1990; 63: 515–524.
38. Stouffer GA, Owens GK. TGF-β promotes proliferation of cultured SMC via both PDGF-AA-dependent and PDGF-AA-independent mechanisms. J Am Coll Cardiol 1994; 93: 2048–2055.

39. Sato M, Ohsaki Y, Tobise K. TGF-β-1 proliferated vascular smooth-muscle cells from spontaneously hypertensive rats. Am J Hypertens 1995; 8: 160–166.
40. Orlandini AM, Ropraz P, Gabbiani G. Proliferative activity and α-smooth muscle actin expression in cultured rat aortic smooth muscle cells are differently modulated by TGF-β-1 and heparin. Exp Cell Res 1994; 214: 528–536.
41. Saltis J, Agrotis A, Bobik A. TGF-β-1 potentiates growth factor-stimulated proliferation of vascular smooth-muscle cells in genetic-hypertension. Am J Physiol 1992; 263: C420–C428.
42. Owens GK, Geisterfer AT, Yang YW, Komoriya A. TGF-β induced growth inhibition and cellular hypertrophy in cultured vascular smooth muscle cells. J Cell Biol 1988; 107: 771–780.